Full scale verification of wind farm production predictions

Larsen, Gunner Chr.; Larsen, Torben J.; Ott, Søren; Hansen, Kurt Schaldemose; Aagaard Madsen , Helge

Published in:
Proceedings of the 23rd International Congress of Theoretical and Applied Mechanics (ICTAM 2012)

Publication date:
2012

DEBONDING ANALYSES IN ANISOTROPIC MATERIALS WITH STRAIN-GRADIENT EFFECTS

Brian Nyvang Legarth*
*Department of Mechanical Engineering, Technical University of Denmark, Kgs. Lyngby, 2800, Denmark

Summary A unit cell approach is adopted to numerically analyze the effect of plastic anisotropy on damage evolution in a micro-reinforced composite. The matrix material exhibit size effects and a visco-plastic anisotropic strain gradient plasticity model accounting for such size effects is adopted. A conventional cohesive law is extended such that both the average as well as the jump in plastic strain across the fiber-matrix interface are accounted for. Results are shown for both conventional isotropic and anisotropic materials as well as for higher order isotropic and anisotropic materials with and without debonding. Generally, the strain gradient enhanced material exhibits higher load carry capacity compared to the corresponding conventional material. A sudden stress drop occurs in the macroscopic stress-strain response curve due to fiber-matrix debonding and the results show that a change in yield stress, which is caused by plastic anisotropy, affects the overall composite failure strain.

INTRODUCTION TO THE PROBLEM

For a composite reinforced at the micron scale, two competing mechanisms affect the overall behavior: (I) interfacial failure reduces the strength and (II) strain-gradient effects enhance the strength. When analyzing such composites in general a full 3D analysis is required in order to fully represent the geometry, the loading and the boundary conditions. Such analyses are complicated and the computations become very time consuming when anisotropic plasticity and progressive debonding is to be accounted for. Thus, assuming a periodical distribution of the reinforcement allows for greatly simplified approaches. Here, a composite material having a periodical distribution of reinforcement is analyzed using a plane strain unit cell approach. Thus, the results presented in this study approximate a composite of rather long, almost aligned, stiff reinforcement which is subjected to a fixed stress state that is acting mainly in the transverse direction of the reinforcement. Fig. 1(a) shows the distribution of fibers and Fig. 1(b) shows the unit cell adopted here. The orthonormal basis, $\mathbf{n}_i$, of the principal axes of plastic anisotropy, $\hat{x}_i$, is defined by the angle θ, from from the global Cartesian coordinate system, x_i. The displacements Δ_1 and Δ_2 are prescribed such that ratio, κ, of the average stress at the cell edges remains constant. Fig. 1(c) shows an example of the finite element mesh adopted. The element type is 8-node elements.

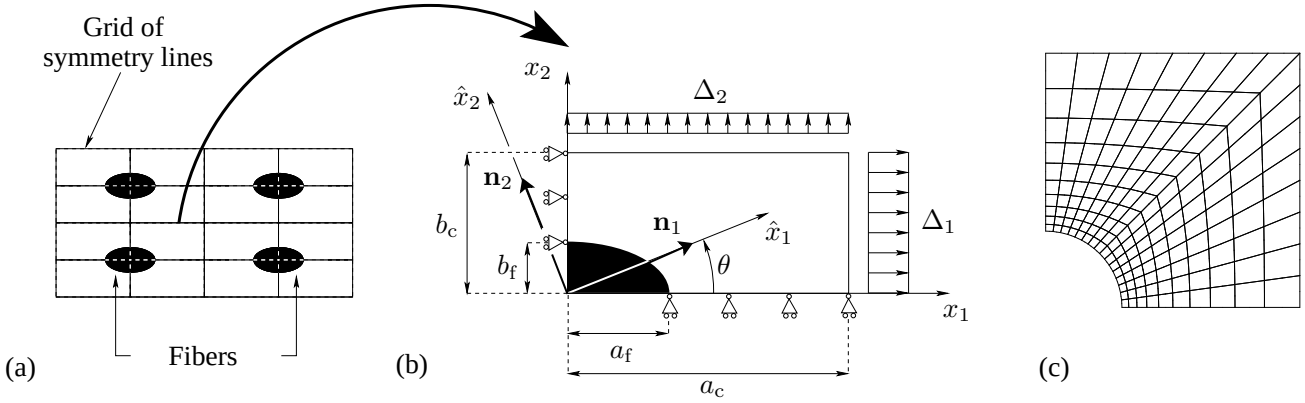

Figure 1. The plane strain cell model for the composite. (a) Periodically distributed fibers. (b) The cell used for modeling with initial dimensions, loads, supports and coordinate systems. (c) Example of finite element mesh using adopted, $\frac{a_f}{b_f} = \frac{a_c}{b_c} = 1$.

MATERIAL MODELS

Higher order elasto-plastic constitutive model

The fibers are assumed to be purely elastic with a stiffness much larger than the elasto-plastic matrix material, which is assumed to obey the strain gradient model proposed by Fleck and Hutchinson [1]. In addition, plastic anisotropy is accounted for using the anisotropic version of the Fleck and Hutchinson model suggested by Legarth [2]. Thus, the effective plastic strain, $\dot{E}^p$, is enriched by the gradients of the conventional effective plastic strain, $\dot{\epsilon}^p$, and a material length scale parameter, l_*, as

$$\dot{E}^p = \sqrt{\frac{2}{3}\dot{\epsilon}^p_{ij}\dot{\epsilon}^p_{ij} + l_*^2 \dot{\epsilon}^{,p}_{,i}\dot{\epsilon}^{,p}_{,i}} \qquad ; \qquad \dot{\epsilon}^p_{ij} = \dot{\epsilon}^p \frac{\partial \Gamma}{\partial \sigma_{ij}} \qquad ; \qquad \dot{\epsilon}^p = \sqrt{\frac{2}{3}\dot{\epsilon}^p_{ij}\dot{\epsilon}^p_{ij}} \tag{1}$$

The work-conjugate effective stress is denoted σ_c and is given in table 1. Plastic anisotropy is accounted for by the classical anisotropic Hill yield surface. For the case of plane strain conditions with $\sigma_{13} = \sigma_{23} = 0$ the yield surface is

$$\Gamma = \sqrt{\tfrac{3}{2(F+G+H)}\left[F(\hat{\sigma}_{22}-\hat{\sigma}_{33})^2 + G(\hat{\sigma}_{33}-\hat{\sigma}_{11})^2 + H(\hat{\sigma}_{11}-\hat{\sigma}_{22})^2 + 2N\hat{\sigma}_{12}^2\right]} \tag{2}$$

where the Cauchy stresses, $\hat{\sigma}_{ij}$, refer to the principal axes of plastic anisotropy. For $F = G = H = 1$ and $N = L = M = 3$, Eq. (2) equals the isotropic Mises yield surface, σ_e. A higher-order stress measure is also introduced as ρ_i.

a) Corresponding author. E-mail: bnl@mek.dtu.dk

	Conventional materials $(l_* = 0, \rho_i = 0)$	Higher order materials $(l_* \neq 0, \rho_i \neq 0)$
Isotropic	$\rho_{i,i} = 0$	$\rho_{i,i} = q - \sigma_{\mathrm{e}}$
$(\Gamma = \sigma_{\mathrm{e}})$	$\sigma_{\mathrm{c}} = \sigma_{\mathrm{e}}$	$\sigma_{\mathrm{c}} = \sqrt{(\sigma_{\mathrm{e}} + \rho_{i,i})^2 + l_*^{-2}\rho_i\rho_i}$
Anisotropic	$\rho_{i,i} = 0$	$\rho_{i,i} = q - \Gamma$
	$\sigma_{\mathrm{c}} = \Gamma$	$\sigma_{\mathrm{c}} = \sqrt{(\Gamma + \rho_{i,i})^2 + l_*^{-2}\rho_i\rho_i}$

Table 1. Summary of the effective stress, σ_{c}, for different materials.

Higher-order cohesive model

The bi-axial loading on the unit cell, Fig. 1, will tend to cause both normal and tangential interfacial separation, u_n and u_t, respectively, at the fiber-matrix interface. The cohesive zone model proposed by Tvergaard [3] takes both types of separation into account and therefore this model may seem suitable for the present study. However, due to the existence of the higher order stress, ρ_i and corresponding higher order tractions, $\rho_i n_i$ additional terms need to be included in order to have a conventional as well as higher order stress-free surface after debonding failure. Hence, a non-dimensional damage parameter is introduces as [4]

$$\lambda = \sqrt{\left(\frac{u_n}{\delta_n}\right)^2 + \left(\frac{u_t}{\delta_t}\right)^2 + l_*^2\left[\left(\frac{<\epsilon^p>}{l_A}\right)^2 + \left(\frac{[\epsilon^p]}{l_J}\right)^2\right]} \tag{3}$$

where $<\epsilon^p>$ is the average (subscript A) and $[\epsilon^p]$ is the *half* jump (subscript J) in plastic strain across the interface, respectively, whereas l_A and l_J are corresponding critical interfacial length scale parameters. For $\lambda \geq 1$ total separation have occurred. It is noted, that since the fiber is taken to be purely elastic, $<\epsilon^p>=[\epsilon^p]$. The corresponding tractions are

$$T_n = \frac{u_n}{\delta_n}F(\lambda) \quad ; \quad T_t = \alpha\frac{u_t}{\delta_t}F(\lambda) \quad ; \quad T_A = l_*^2\frac{\delta_n}{l_A^2}F(\lambda)<\epsilon^p> \quad ; \quad T_J = l_*^2\frac{\delta_n}{l_J^2}F(\lambda)[\epsilon^p] \tag{4}$$

with $\alpha = \delta_n/\delta_t$ and $F(\lambda) = \frac{27}{4}\sigma_{max}(1 - 2\lambda + \lambda^2)$ for $0 \leq \lambda \leq 1$. The maximum interfacial stress is denoted σ_{max}.

RESULTS AND CONCLUSION

Fig. 2 shows results for a load case with $\kappa = \frac{\sigma_2}{\sigma_1} = 0.5$ corresponding to bi-axial plane strain tension. The fiber volume fraction is $V_f = \frac{\pi a_f b_f}{4 a_c b_c}$, with $\frac{a_f}{b_f} = \frac{a_c}{b_c} = 1$. The initial yield stress is $\sigma_0/E = 0.003$, where E is Young's modulus. The coefficients of anisotropy are $F = 0.7, G = 3.33, H = 1$ and $N = 9.6$ with $\theta = 0^o$ and $\sigma_{max} = 3\sigma_0$.

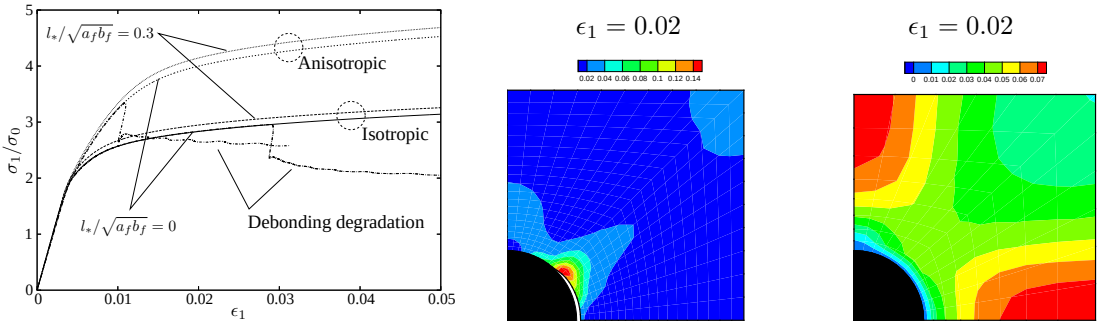

(a) (b) (c)

Figure 2. Bi-axial tension results, $\kappa = 0.5$. (a) Average stress-strain curves (b) Contours of effective plastic strain for a conventional anisotropic material with debonding (c) Contours of effective plastic strain for a higher order anisotropic material without debonding.

For both isotropic and anisotropic behavior the effect of the material length scale parameter, l_*, is an increased load carrying capacity, Fig. 2(a). A sudden stress drop occurs due to debonding, Fig. 2(a), and in Fig. 2(b) the corresponding void at the fiber-matrix interface is shown. Fig. 2(c) illustrates, that at the fiber-matrix interface the plastic strain is suppressed and the strain is smaller compared to the conventional case with severe plastic deformations at the tip of the void, Fig. 2(b).

In conclusion, this study analyzes numerically the combined effects of plastic anisotropy, size-effects and debonding in a composite material. Debonding is seen as a sudden stress drop and plastic anisotropy highly affects the failure strain, while the size-effect is observed as an increased load carrying capacity.

References

[1] Fleck. N. A., Hutchinson, J. W.: A reformulation of strain gradient plasticity. *J. of the. Mech. and Phys. of Solids.* **49** 2245–2271, 2001.
[2] Legarth, B. N.: Strain-gradient effects in anisotropic materials. *Model. and Sim. in Mater. Sci. and Eng.* **15**:S71–S81, 2007.
[3] Tvergaard, V.: Effect of fibre debonding in a whisker-reinforced metal. *Mater. Sci. & Eng.* **A125**:203–213, 1990.
[4] Niordson, C. F.: Cohesive element for Fleck & Hutchinson 2001. *Technical report*, Technical University of Denmark, 2010.